

Article

# Reworking of Eoarchean to Mesoarchean Continental Crust in the Anshan–Benxi Area, North China Craton—Evidence from Lianshanguan ca. 2.5 Ga Syenogranites

Wen Zhang \* , Wei Wang, Lilin Du, Pinghua Liu and Wang Xu 

Institute of Geology, Chinese Academy of Geological Sciences, Beijing 100037, China

\* Correspondence: wzhan7@126.com

**Abstract:** The Anshan–Benxi area, situated in the northeast of the North China Craton (NCC), is home to not only the oldest rocks in China (~3.8 Ga) but also a diverse range of granitoids dated between 3.8 and 2.5 Ga. The Lianshanguan batholith, covering an area of approximately 250 km<sup>2</sup> with an east–west trend, predominantly consists of syenogranites ( $K_2O > 4$  wt. % and  $K_2O/Na_2O$  ratios > 1.3). Laser ablation inductively coupled plasma mass spectrometry (LA-ICP-MS) U-Pb analyses of the two syenogranites yielded concordant ages of  $2541 \pm 22$  and  $2512 \pm 13$  Ma, respectively. These syenogranites had zircon  $\epsilon_{Hf}(t)$  values ranging from –20 to +4.9 with two-stage Hf model ages ( $T_{DM2}(Hf)$ ) spanning 3.9–2.7 Ga. Based on petrological, geochemical, and isotopic characteristics, we conclude that the Lianshanguan syenogranites are mainly resulted from the reworking of complicated Eoarchean–Mesoarchean crustal materials, possibly with a small proportion of ~2.7 Ga juvenile crustal materials. When compared with coeval syenogranites from the Northern Liaoning and Western Liaoning–Eastern Hebei areas, ~2.5 Ga syenogranites from the Anshan–Benxi area displayed more complicated  $T_{DM2}(Hf)$  ages, hinting at a pronounced late Neoarchean reworking of the Eoarchean to Mesoarchean continental crust (including metasedimentary sources) primarily in the Anshan–Benxi region of the North China Craton. This scenario significantly bolsters the arc–continent collision model.



**Citation:** Zhang, W.; Wang, W.; Du, L.; Liu, P.; Xu, W. Reworking of Eoarchean to Mesoarchean Continental Crust in the Anshan–Benxi Area, North China Craton—Evidence from Lianshanguan ca. 2.5 Ga Syenogranites. *Minerals* **2024**, *14*, 5. <https://doi.org/10.3390/min14010005>

Academic Editor: Pierre Schiano

Received: 9 November 2023

Revised: 8 December 2023

Accepted: 14 December 2023

Published: 19 December 2023



**Copyright:** © 2023 by the authors. Licensee MDPI, Basel, Switzerland. This article is an open access article distributed under the terms and conditions of the Creative Commons Attribution (CC BY) license (<https://creativecommons.org/licenses/by/4.0/>).

## 1. Introduction

The geodynamic regime of the early Precambrian continental evolution has long been a focal point in geology. Hadean and Eoarchean rocks and zircons have been identified in different cratons, such as Slave, North Atlantic, North China, Kaapvaal, Pilbara, and Yilgarn (e.g., [1–20]). Studies of whole-rock Nd isotopes and zircon Hf isotopes of Hadean to Archean rocks have indicated that more than 70% of the continental crust was derived from the mantle before 2.5 Ga [21]. Therefore, new discoveries in this area are crucial for the study of early continental crust formation and evolution [22].

The NCC, the largest craton in China, has 3.8 Ga rocks and numerous Hadean to Paleoarchean zircons [3,9,22–26]. Globally, the formation and reworking of the continental crust are primarily marked by three igneous age peaks at approximately 2.9, 2.7, and 2.5 Ga [27]. In the NCC, the intense tectonic–magmatic activity during the late Neoarchean (~2.6 to 2.5 Ga) provides valuable insights into key geodynamic processes, as it includes evidence supporting both vertical and horizontal tectonic hypotheses [28,29]. The distinct geochemical signatures in the Neoarchean rocks offer critical insights into the temporal evolution and dynamics of these contrasting geodynamic models. This, combined with the NCC’s well-preserved geological record, makes it an ideal region for studying the formation and evolution of the Earth’s early continental crust.

In this study, we focus on the Neoarchean Lianshanguan pluton in the Anshan–Benxi area, which is characterized predominantly by syenogranites. Through using new whole-rock geochemical and zircon U-Pb ages and Lu-Hf isotope analyses of the Lianshanguan pluton, we aim to uncover more about the genesis of the ~2.5 Ga syenogranites and constrain the reworking of the Eoarchean to Mesoarchean continental crust throughout the Earth's geological history. Furthermore, through comparing our results with existing data from other late Neoarchean granites in the Anshan–Benxi, Northern Liaoning and Western Liaoning–Eastern Hebei areas, we can significantly expand our understanding of crustal evolution during the late Neoarchean (Figure 1).

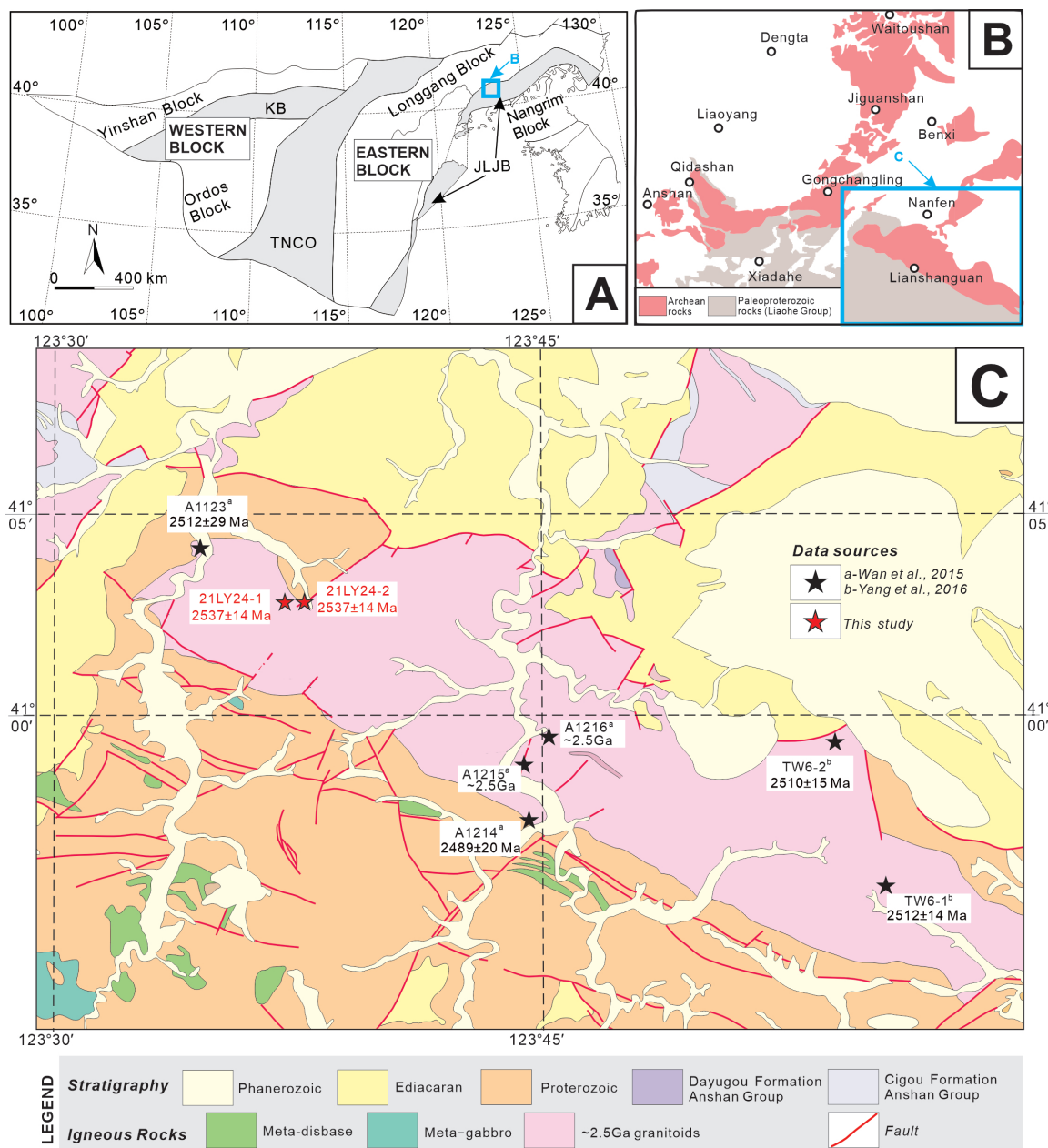


**Figure 1.** (A) Tectonic framework of NCC (modified after [30]), KB—Khondalite Belt; TNCO—Trans North–Central Orogen; JLJB—Jiao-Liao-Ji Belt; (B) Geological map of the Anshan–Benxi area in the Eastern Block, North China Craton (modified after [31,32]); (C) A simplified geological map of the Lianshanguan pluton in the Anshan–Benxi area (after [32,33]). (Our data and data from Wan et al., 2015 [31] and Yang et al., 2016 [33]).

## 2. Geological Background

The Anshan–Benxi area, situated in the northeast of the NCC, boasts not only China's oldest rocks (~3.8 Ga) [9,10,34–38] but also the most widely distributed Mesoarchean potassic granitoid pluton [39–41]. The area includes various granites from 3.8 to 2.5 Ga, such as the 3.8–3.1 Ga Bajiafen, Dongshan, Shengousi, and Guodishan Complexes, the 3.3–3.1 Ga Chentaigou granite, the 3.1 Ga Lishan trondhjemite, the 3.0 Ga Donganshan–Jinjialing trondhjemitic to monzogranitic gneisses, the 3.0–2.9 Ga Tiejiashan–Gongchangling K-rich granite, and the 2.5 Ga Qidashan syenogranite and Lianshanguan granite [9,23,34,37,39,40,42–44].

The Lianshanguan pluton, located in the Anshan–Benxi area and extending in an east–west direction with an area of ~250 km<sup>2</sup>, occurs as a batholith, and includes BIF, plagioclase amphibolite, and Anshan Group gneiss as xenoliths. The pluton is unconformably overlain by the Paleoproterozoic Langzishan Formation (Liaohe Group), and the contact area has become a ductile deformation zone. In a previous regional geological report [32], the pluton was defined as migmatite. However, through field investigation, it was discovered that the main rock type of the pluton was granite, and it was only migmatized at the margin.

Several zircon U–Pb ages of the Lianshanguan pluton have been reported (Table 1): 2563 ± 3 Ma for gneissic biotite monzogranite [45], 2511 ± 15 Ma and 2540 ± 25 Ma for flesh-red K-feldspar granite (065-1 and 093-2) [46], 2533 ± 42 Ma for gray–white remelted migmatite (090-1) [46], 2489 ± 20 Ma for weakly deformed syenogranite (A1214) [31], 2512 ± 29 Ma for gneissic syenogranite (A1123) [31], 2512 ± 14 Ma for light-flesh-red syenite (TW6-1) [33], 2510 ± 15 Ma for gray–white streaked monzogranite (TW6-2) [33], 2493 ± 130 Ma for medium-fine grained K-feldspar granite (16LSG66-2) [47], and 2484 ± 29 Ma for flesh-red K-feldspar granitic pegmatite vein (15LSG43-1) [47]. In addition, a recent regional geological report [45] pointed out that the rock types of the Lianshanguan pluton are gneissic porphyritic biotite monzogranite and gneissic biotite monzogranite.

**Table 1.** Summary of zircon age data for Lianshanguan granites, Anshan–Benxi area, North China Craton.

Sample No.	Age (Ma)	Rock Type <sup>1</sup>	References
21LY24-1	2541 ± 22	flesh-red fine-grained syenogranite	This study
21LY24-2	2517 ± 7	gray–white medium-grained syenogranite	This study
16LSG66-2	2493 ± 130	medium-fine grained K-feldspar granite	[47]
15LSG43-1	2484 ± 29	flesh-red K-feldspar granitic pegmatite vein	[47]
TW6-1 <sup>2</sup>	2512 ± 14	light-flesh-red syenite	[33]
TW6-2 <sup>3</sup>	2510 ± 15	gray–white streaked monzogranite	[33]
A1214	2489 ± 20	weakly deformed syenogranite	[31]
A1123	2512 ± 29	gneissic syenogranite	[31]
065-1	2511 ± 15	flesh-red K-feldspar granite	[46]
093-2	2540 ± 25	flesh-red K-feldspar granite	[46]
090-1	2533 ± 42	gray–white remelted migmatite	[46]
Unknown	2563 ± 3	gneissic biotite monzogranite	[45]

Notes: <sup>1</sup> There is considerable variation in rock types due to the application of diverse classification criteria. <sup>2</sup> Four distinct samples (Ls611–614) were chosen for major and trace element analyses for TW6-1. <sup>3</sup> Four distinct samples (Fj621–624) were chosen for major and trace element analyses for TW6-2.

## 3. Sampling and Petrography

Lianshanguan granite samples were collected from the south of Chenjia Village in Tianshui Country, Liaoyang Town, Liaoyang City, Liaoning Province (Figure 1).

Sample 21LY24-1 (41°02'44.29'' N, 123°37'06.10'' E) is a flesh-red, fine-grained, muscovite-bearing, potassium-rich granite. The main minerals are K-feldspar (30–50 vol. %, mainly microcline, perthite, and orthoclase), plagioclase (10–20 vol. %), quartz (20–30 vol. %), muscovite (8–10 vol. %), and biotite (few, mostly altered to chlorite) (Figure 2). Accessory minerals include zircon and apatite. Little opaque minerals are also observed.

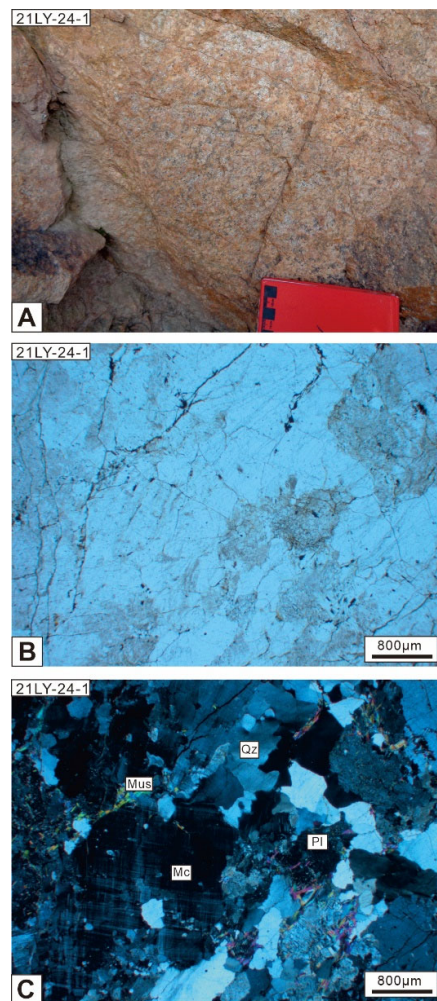


**Figure 2.** (A) Representative photographs of the Lianshanguan syenogranites outcrop in the Anshan–Benxi area. (B,C) Thin-section microphotographs of representative Lianshanguan syenogranites. Abbreviations: Qz—quartz, Pl—plagioclase, Mc—microcline, Mus—Muscovite.

Sample 21LY24-2 ( $41^{\circ}03'00.31''$  N,  $123^{\circ}37'27.64''$  E) is a gray–white, medium-grained, potassium-rich granite. The main minerals are K-feldspar (40–60 vol. %, mainly microcline, perthite, and orthoclase), plagioclase (10–25 vol. %, sericitization occurs), quartz (20–30 vol. %, mostly recrystallized), and some muscovite and biotite (Figure 2).

#### 4. Analytical Methods

Cathodoluminescence (CL) was carried out using a TESCAN Field Emission Scanning Electron Microscope (TESCAN Mira3, TESCAN company, Brno, Czech Republic) at the facility of Nanjing Hongchuang Exploration Technology Service Co., Ltd. U-Pb dating and trace element analysis of zircon were undertaken using LA-ICP-MS at the Wuhan Sample Solution Analytical Technology Co., Ltd. in Wuhan, China. The specifics of the operating conditions and data processing are detailed in Zong et al. [48]. For this study, the laser's spot size and pulse frequency were adjusted to  $30\text{ }\mu\text{m}$  and 5 Hz, respectively. The external standards for U-Pb dating and trace element analysis calibration were zircon 91,500 and glass NIST610. Plesovic [49] and GJ-1 [50] were employed as unknown samples to limit stability and accuracy. ICPMSDataCal software (version 10.9, China University of Geosciences, Wuhan, China) was used to perform offline selection and integration of background and analyzed signals, time-drift correction, and quantitative calibration [51,52]. Concordia diagrams and weighted mean calculations were performed using Isoplot/Ex\_ver3 [53], as elaborated in Supplementary Table S1.

In situ analyses of Hf isotope ratios were performed using a RESOlution LR laser-ablation system (Canberra, Australia) coupled with a Nu Plasma II MC-ICP-MS (Wrexham, Wales, UK) at the Nanjing FocuMS Technology Co. Ltd., Nanjing, China. A 193 nm ArF excimer laser, homogenized by a set of beam delivery systems, targeted the zircon surfaces with a fluence of  $4.5 \text{ J/cm}^2$ . The procedure involved a 20-s background (gas blank) measurement, followed by a 40-s analysis at a spot diameter of  $50 \mu\text{m}$  and a repetition rate of 9 Hz. Helium ( $370 \text{ mL/min}$ ) served as the carrier gas to effectively transfer aerosols from the ablation cell, mixing with argon ( $\sim 0.97 \text{ L/min}$ ) via a T-connector before entering the ICP torch. The integration interval for the Nu Plasma II was set at 0.3 s (equating to 133 cycles during the 40 s). Standard zircons such as GJ-1, 91,500, Plešovice, Mud Tank, and Penglai were utilized for quality control for every fifteen unknown samples. The results are presented in Supplementary Table S2.

Major and trace elements analyses of the whole rock were conducted using X-ray fluorescence (XRF) (Primus II, Rigaku, Japan) and Agilent 7700e ICP-MS, respectively, at the Wuhan Sample Solution Analytical Technology Co., Ltd. in Wuhan, China. The results are provided in Supplementary Table S3.

## 5. Results

### 5.1. Zircon U-Pb Dating

Zircon grains from samples 21LY24-1 and 21LY24-2 are mostly euhedral to subhedral and translucent. The grains' lengths range from 80 to 120  $\mu\text{m}$ , with aspect ratios of 2:1–3:2. CL images reveal that most zircons have a core-rim texture (see Figure 3), but some exhibit strong recrystallization or cracking. Some cores have igneous oscillatory growth zones [54,55], while others do not show a clear igneous texture, possibly indicating partial resetting during metamorphism. Some rims are gray or dark with no zoning, indicating a metamorphic origin [56]. Analyses were performed on oscillatory zonings or other cores.

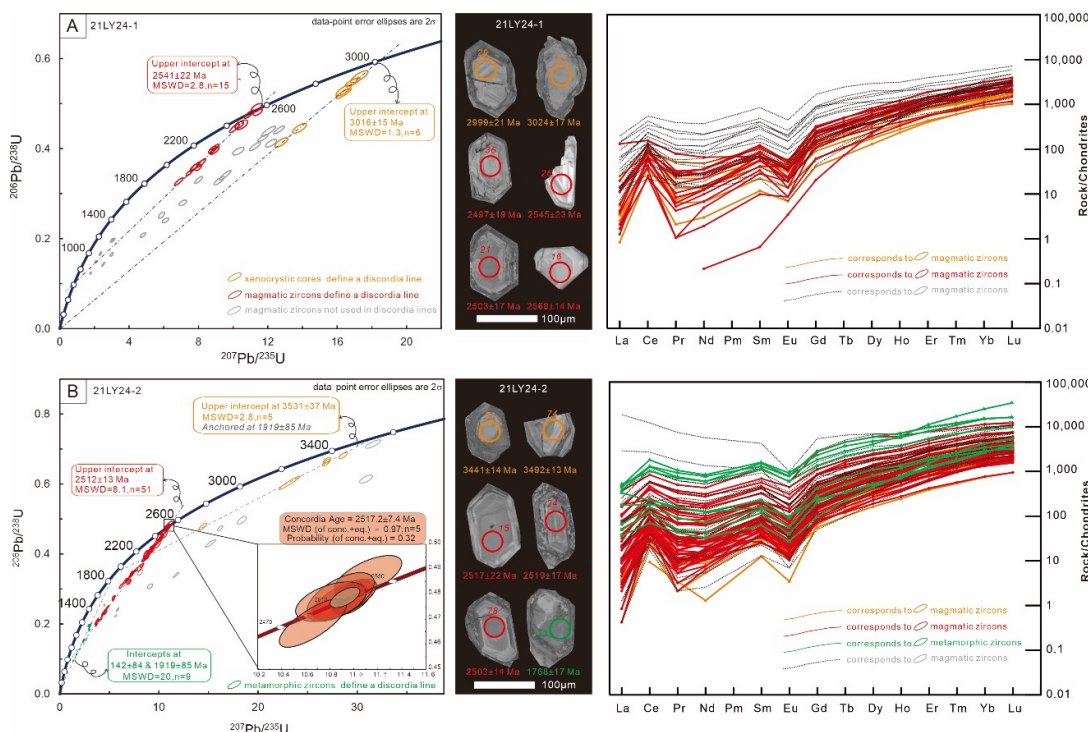


**Figure 3.** U-Pb inverse concordia diagrams, representative zircon CL images and chondrite-normalized zircon REEs for Lianshanguan syenogranite samples (A) 21LY24-1 and (B) 21LY24-2 (values after [57]).

Sample 21LY24-1: Forty-one analyses on magmatic cores show severe Pb loss, with some cores yielding low Th/U ratios (<0.1). Fifteen analyses on zircon cores define a discordia line with an upper intercept at  $2541 \pm 22$  Ma (MSWD = 2.8), which is interpreted as the emplacement age of the sample. Six analyses on xenocrystic cores define a discordia line with an upper intercept at  $3016 \pm 15$  Ma (MSWD = 1.3). Other analyses yielded  $^{207}\text{Pb}/^{206}\text{Pb}$  ages from  $1628 \pm 23$  to  $2943 \pm 19$  Ma with a discordance ( $|(^{207}\text{Pb}/^{206}\text{Pb}$  age)/( $^{206}\text{Pb}/^{238}\text{U}$  age) – 1)  $\times 100\%$ ) of 20–137, indicating significant Pb loss.

Sample 21LY24-2: Eighty-three analyses on magmatic cores show severe Pb loss, with some cores yielding low Th/U ratios (<0.1). Fifty-one analyses on zircon cores define a discordia line with an upper intercept at  $2512 \pm 13$  Ma (MSWD = 8.1), and five analyses close to concordia yield a concordant age of  $2517 \pm 7$  Ma (MSWD = 0.97), representing the crystallization age of sample 21LY24-2. Nine analyses define a discordia line with intercepts at  $142 \pm 84$  and  $1919 \pm 85$  Ma (MSWD = 20), and we interpret the upper age of  $1919 \pm 85$  Ma as the metamorphic age of the sample. If anchored at this metamorphic age, five analyses on xenocrystic cores define a discordia line with an upper intercept at  $3531 \pm 37$  Ma (MSWD = 2.8). Other analyses yielded  $^{207}\text{Pb}/^{206}\text{Pb}$  ages from  $1934 \pm 19$  to  $3569 \pm 11$  Ma with high discordance, indicating significant Pb loss.

### 5.2. Zircon Hf Isotopic Composition

Zircon grains from sample 21LY24-1 underwent thirty-four Hf analyses. Fourteen of these analyses were calculated at a crystallization age of  $2541 \pm 22$  Ma and yielded  $\varepsilon_{\text{Hf}}(t)$  values ranging from –13.0 to +4.9 (Figure 4A) and depleted-mantle two-stage Hf model ages ( $T_{\text{DM2}}(\text{Hf})$ ) of 2695–3569 Ma (Figure 4B). Six analyses, calculated at the age of  $3016 \pm 15$  Ma, yielded  $\varepsilon_{\text{Hf}}(t)$  values of –2.7 to +0.6 and  $T_{\text{DM2}}(\text{Hf})$  ages of 3295–3554 Ma. Other analyses were calculated at their apparent ages (2520–2943 Ma) and yielded  $\varepsilon_{\text{Hf}}(t)$  values of –12.5 to +3.4 and  $T_{\text{DM2}}(\text{Hf})$  values of 2845–3775 Ma.

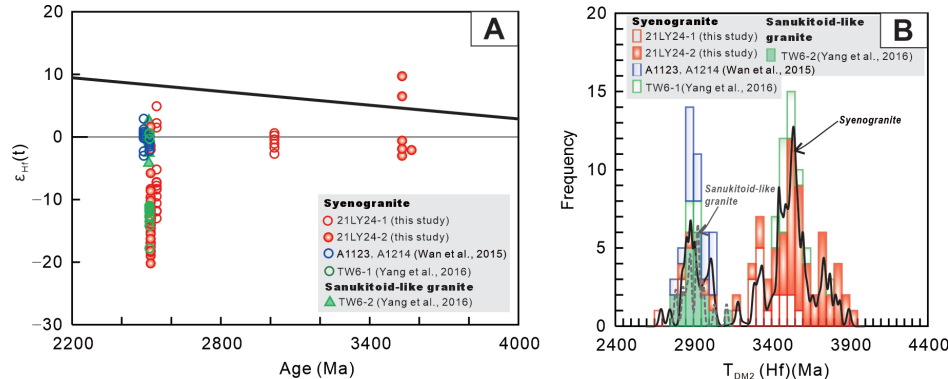


**Figure 4.** (A) Zircon  $\varepsilon_{\text{Hf}}(t)$  versus crystallization age; (B) Distribution of two-stage Hf model ages ( $T_{\text{DM2}}$ ).  $T_{\text{DM2}}$  is defined in Supplementary Table S2. Please note that the analyses calculated based on apparent ages are not included in this figure. (Our data and data from Wan et al., 2015 [31] and Yang et al., 2016 [33]).

Seventy-five Hf analyses were carried out on zircon grains from sample 21LY24-2. Forty-nine of these analyses were calculated at a crystallization age of  $2517 \pm 7$  Ma and yielded  $\varepsilon_{\text{Hf}}(t)$  values ranging from –20.2 to +1.6 (Figure 4B) and  $T_{\text{DM2}}(\text{Hf})$  ages of 2838–3900 Ma (Figure 4B). Five analyses, calculated at the age of  $3531 \pm 37$  Ma, yielded  $\varepsilon_{\text{Hf}}(t)$  values of –3.0 to +9.7 and  $T_{\text{DM2}}(\text{Hf})$  ages of 3295–3554 Ma. Other analyses with apparent ages (2555–3771 Ma) yielded  $\varepsilon_{\text{Hf}}(t)$  values of 0.3 to 1.0 and  $T_{\text{DM2}}(\text{Hf})$  values of 2801–4149 Ma. The rest of the analyses with apparent ages (1695–2068 Ma) yielded  $\varepsilon_{\text{Hf}}(t)$  values of –34.5 to –22.7 and  $T_{\text{DM2}}(\text{Hf})$  values of 3533–4055 Ma. It is worth noting that in this study, we used an upper continental crustal reservoir with  $^{176}\text{Lu}/^{177}\text{Hf} = 0.0093$  [58] instead of an average continental crustal reservoir with  $^{176}\text{Lu}/^{177}\text{Hf} = 0.015$  [59] (which would produce ages of ~0.2 Ga younger).

### 5.3. Geochemistry

Lianshanguan granites have  $K_2O$  concentrations greater than 4 wt. % and  $K_2O/Na_2O$  ratios greater than 1.3, which Wan et al. [37] defined as syenogranites (Figure 5A,B). In the QAP diagram, Lianshanguan samples also plot in the field of syenogranite [60]. These syenogranites have  $SiO_2$  contents ranging from 71.08 to 75.32 wt. %,  $Al_2O_3$  contents ranging from 12.97 to 14.18 wt. %,  $Na_2O + K_2O$  contents ranging from 8.7 to 9.8 wt. %, and Mg# values ranging from 20.4 to 49.7. They are alkalic to alkali-calcic [61] and slightly peraluminous to peraluminous ( $ASI = 1.08\text{--}1.18$ ) (Figure 5). Chondrite-normalized REE patterns reveal enrichment in LREEs [ $(La/Yb)_N = 2.6\text{--}60.6$ ] and negative Eu anomalies ( $\delta Eu = 0.21\text{--}0.39$ ) (Figure 5G). Primitive mantle-normalized multi-element patterns show enrichments in Th, K, Pb, and Nd, and depletions in Ba, Nb, Ta, P, and Ti (Figure 5H).

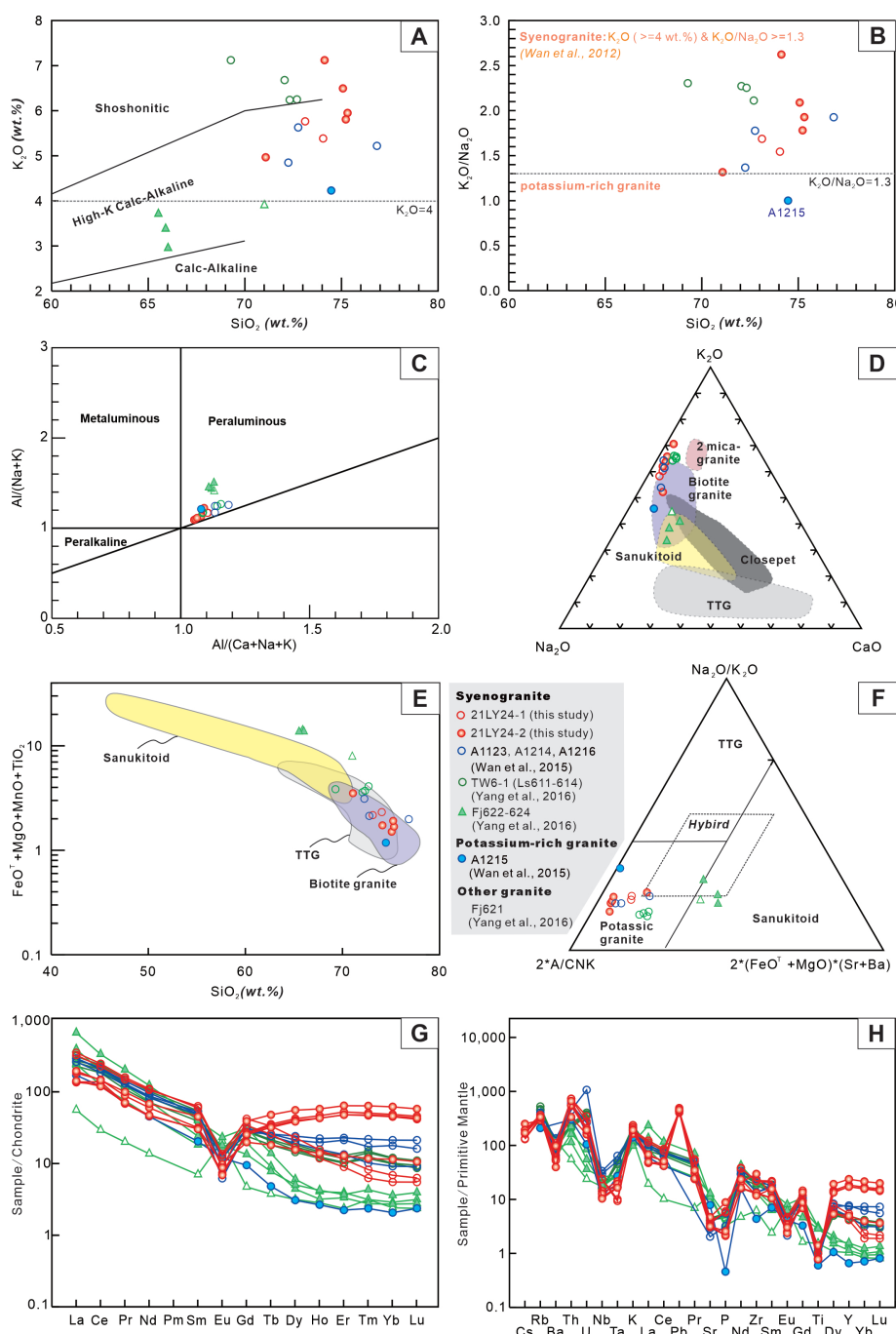


**Figure 5.** (A)  $K_2O$ - $SiO_2$  classification diagram (after [62]). (B)  $K_2O/Na_2O$ - $SiO_2$  classification diagram (after [37]). (C) A/NK-A/CNK diagram [molar  $Al_2O_3/(Na_2O + K_2O)$  versus molar  $Al_2O_3/(CaO +$

$\text{Na}_2\text{O} + \text{K}_2\text{O}]$  (after [11]). (D)  $\text{K}_2\text{O}-\text{Na}_2\text{O}-\text{CaO}$  diagram (after [63]). (E)  $(\text{FeO}^\text{T} + \text{MgO} + \text{MnO} + \text{TiO}_2)$  vs.  $\text{SiO}_2$  diagrams (after [64]). (F)  $\text{Na}_2\text{O}/\text{K}_2\text{O}-2\text{A}/\text{CNK}-2(\text{FeO}^\text{T} + \text{MgO})(\text{Sr} + \text{Ba})$  (after [55]). (G) Chondrite-normalized REEs (values after [57]). (H) Primitive mantle-normalized trace elements (values after [57]). (Our data and data from Wan et al., 2015 [31] and Yang et al., 2016 [33]).

## 6. Discussions

### 6.1. Magmatic Emplacement Age of Granites

The two syenogranites from this study have ages of  $2541 \pm 22$  Ma (sample 21LY24-1) and  $2517 \pm 7$  Ma (sample 21LY24-2). Combined with data from previous studies, the crystallization age of the Lianshanguan syenogranite is constrained to between 2.49 and 2.56 Ga ([31,46,47] and this study), and the formation age of the monzogranite is limited to 2.51 Ga [33].

The age of  $1919 \pm 85$  Ma obtained from sample 21LY24-2 is consistent with the widely distributed metamorphism of the Jiao-Liao-Ji Belt at around 1.83–1.95 Ga [65–74]. However, it is worth noting that while the Anshan–Benxi area indeed documents this late Paleoproterozoic metamorphic occurrence, the main preserved metamorphic event in this area occurred at 2.5 Ga [75]. The lower intercept (142 Ma) possibly indicates that the pluton could have been largely affected by the destruction of the North China Craton, which culminated at the Early Cretaceous (e.g., [76]).

Due to the disturbance of the zircon U-Pb dating system and analytical errors, it is difficult to determine whether the Lianshanguan granites were formed in a single magmatic event or a series of closely spaced events. Contacts between different granite phases are not clear in the outcrop, and the Lianshanguan granites may have different phases that are indistinguishable in age.

### 6.2. Petrogenesis

To achieve a comprehensive understanding of the Lianshanguan pluton, we integrated samples 21LY24-1 and 21LY24-2 with published data from [31] for samples A1123, A1214, A1215, and A1216, as well as samples TW6-1 and TW6-2 from [33]. Using the Ab-An-Or diagram, we found that all the samples fell into the granite field.

Most of the Lianshanguan granites are syenogranites (21LY24-1, 21LY24-2, A1123, A1214, A1216, and TW6-1). One sample, A1215, has a  $\text{K}_2\text{O}$  concentration greater than 4 wt. % but a  $\text{K}_2\text{O}/\text{Na}_2\text{O}$  ratio less than 1.3, which Wan et al. [37] defined as potassium-rich granite (Figure 5B). From the TW6-2 group, four samples were identified as monzogranites [33]. Specifically, three of them have  $\text{SiO}_2$  concentrations of 65.53–66.03 wt. %,  $\text{Na}_2\text{O}/\text{K}_2\text{O}$  ratios of 1.0–1.2, high  $\text{MgO}$  (2.37–2.56 wt. %) and  $\text{FeO}^\text{T}$  (10.22–10.57 wt. %) with  $\text{Mg}^#$  ranging from 48.0–49.7,  $\text{Ba}+\text{Sr}$  concentrations are 662–887 ppm, and  $(\text{Gd}/\text{Er})_\text{N}$  ratios are 3.6–8.0. These characteristics are similar to the definition of a sanukitoid by Heilimo et al. [77], which includes  $\text{SiO}_2 = 55\text{--}70$  wt. %,  $\text{Na}_2\text{O}/\text{K}_2\text{O} = 0.5\text{--}3$ ,  $\text{MgO} = 1.5\text{--}9$  wt. %,  $\text{Mg}^# = 45\text{--}65$ ,  $\text{K}_2\text{O} = 1.5\text{--}5.0$  wt. %,  $\text{Ba}+\text{Sr} > 1400$  ppm, and  $(\text{Gd}/\text{Er})_\text{N} = 2\text{--}6$ . Furthermore, these sanukitoid-like granites plot in the sanukitoid field in the  $\text{K}_2\text{O}-\text{Na}_2\text{O}-\text{CaO}$  ternary diagram (after [63]) (Figure 5D) and in the 2A/CNK– $\text{Na}_2\text{O}/\text{K}_2\text{O}-2(\text{FeO}^\text{T} + \text{MgO})(\text{Sr} + \text{Ba})$  ternary diagram (Figure 5F).

Due to limited reported data on potassium-rich granite and sanukitoid-like granites, we primarily focused on the petrogenesis of syenogranites in this study. The Lianshanguan syenogranites exhibit low LOI values (0.35–1.05 wt. %), and their  $\text{SiO}_2$ ,  $\text{MgO}$ ,  $\text{FeO}^\text{T}$ ,  $\text{CaO}$ ,  $\text{P}_2\text{O}_5$ , REEs, Y, Ba, Ti, Hf, and Sr show relatively good linear correlation with alteration sensitive Zr (Supplementary Figure S1), indicating their immobility and usability for further discussion. However, some elements such as Th, Ta, Nb, Rb, and Cs display scattered trends with Zr, reflecting remobilization during post-emplacement events.

As previously mentioned, the Late Neoarchean Lianshanguan syenogranites belong to the high-K calc-alkaline to shoshonitic series and are peraluminous, with high  $\text{SiO}_2$  contents

and low mafic oxide contents, indicating little or no contribution from mantle-derived materials to their genesis. On the  $\text{Al}_2\text{O}_3/(\text{FeO}^\text{T} + \text{MgO})$ - $3\text{CaO}-5\text{K}_2\text{O}/\text{Na}_2\text{O}$  diagram, the Lianshanguan syenogranites are consistent with experimental partial melts from metasediments (Figure 6A). This is further supported by the lower  $\text{CaO}/(\text{MgO}+\text{FeO}^\text{T})$  ratios (Figure 6B). Experiments on partial melting have confirmed that mature pelitic sediments can produce peraluminous and potassic granitic melts [78,79].

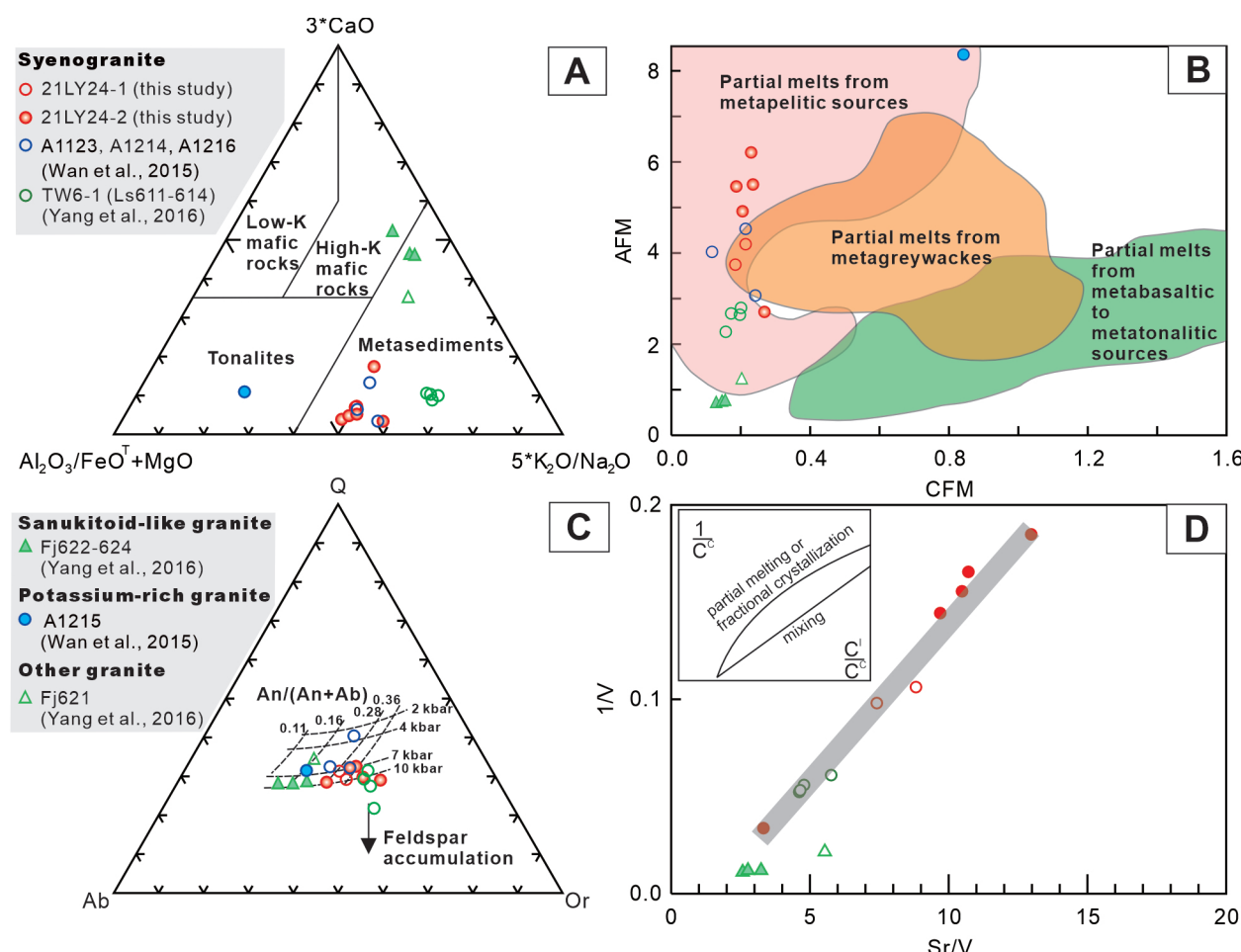


**Figure 6.** Petrogenetic diagrams. (A)  $3\text{CaO}-\text{Al}_2\text{O}_3/(\text{FeO}^\text{T} + \text{MgO})-5\text{K}_2\text{O}/\text{Na}_2\text{O}$  (after [64]). (B) AFM-CFM diagram [molar  $\text{Al}_2\text{O}_3/(\text{FeO}^\text{T} + \text{MgO})$ ] versus molar  $\text{CaO}/(\text{FeO}^\text{T} + \text{MgO})$ ] (after [80]). (C) Q-Ab-Or diagram. (D)  $1/\text{V}$  versus  $\text{Sr}/\text{V}$  diagram. The inset is a schematic of the  $1/\text{C}^c$  versus  $\text{C}^l/\text{C}^c$  diagram (I and C being incompatible and compatible elements, respectively), showing trends produced via magma mixing, fractional crystallization, and partial melting processes (after [81]). (Our data and data from Wan et al., 2015 [31] and Yang et al., 2016 [33]).

The zircon saturation temperatures ( $T_{\text{Zr}}$ ) for the Lianshanguan syenogranites were calculated to vary between 857 and 775 °C, with an average of 809 °C [82], which is slightly lower than the 830 °C observed for A-type granite [83]. The strongly peraluminous compositions, low  $1000 \times \text{Ga}/\text{Al}$  ratios,  $\text{Zr} + \text{Nb} + \text{Ce} + \text{Y}$  contents, existence of Al-rich minerals (such as muscovite), and high normative contents of CIPW corundum (mostly >1%) suggest that they are similar to S-type granites derived from mature pelitic sediments [84,85]. The negative Eu anomalies reflect plagioclase fractionation crystallization and lower melting pressures (Figure 6C). In the  $1/\text{V}$ - $\text{Sr}/\text{V}$  diagram, the Lianshanguan syenogranites define a line with a positive slope, suggesting that their compositional variation could potentially be attributed to mixing processes [81] (Figure 6D). This is also supported by their Hf isotopic compositions. The Lianshanguan syenogranites have variable zircon  $T_{\text{DM2}}(\text{Hf})$  values ranging from 3.90 to 2.70 Ga, which are divided into two groups:

$T_{DM2}$  (Hf) = ~3.90–3.19 Ga with negative  $\epsilon_{Hf}(t)$  ranging from –5.2 to –20.19. This group has a dominant  $T_{DM2}$  (Hf) peak at 3.54 Ga and subordinate age peaks at 3.45, 3.79, 3.74, and 3.34 Ga. A ~3.53 Ga upper intercept age was also obtained in this study (sample 21LY24-2). In addition, a ~3.45 Ga continent microblock was proposed to exist in the Beitai–Waitousha area located in the north of the Lianshanguan area [86]. The Anshan–Benxi area also has ~3810 Ma Baijiafen banded trondhjemite rocks, ~3790 Ma quartz diorite gneisses at Dongshan, 3800 and 3300 Ma migmatites at Dongshan, 3362–3342 Ma Chentaigou supracrustal rocks, and ~3300 Ma Chentaigou granite [9,10,34–38,43]. Dong et al. [39] also highlighted the likelihood of the presence of undiscovered rocks older than 3.3 Ga of varying types in the Anben area, which are anticipated to exhibit relatively higher ratios of  $K_2O/Na_2O$  and elevated  $\sum REE$  contents when compared to the known Paleo- to Eoarchean rocks in the same region. This indicates the involvement of ancient continental crustal materials in their generation.

$T_{DM2}$  (Hf) = ~3.04–2.70 Ga with slightly negative–positive  $\epsilon_{Hf}(t)$  ranging from –3.0 to +4.9, with an average of 0.0. This group has a prominent peak at 2.89 Ga and a subordinate age peak at 3.02 Ga. In addition, the  $T_{DM2}$  (Hf) of one sanukitoid-like granite has similar values, with a dominant peak at 2.93 Ga. To the west of the Lianshanguan granite, there are ~2.9 Ga Tiejiashan-Gongchangling high-K granitoid gneisses, and ~3.0 Ga Dong'anshan granite and Jinjialing trondhjemite gneisses [34,39,40]. The Dagushan BIFs and related supracrustal wall rocks are believed to have formed before 2.99 Ga, indicating that crustal sources extracted from the mantle during the Mesoarchean were involved in their generation [87].

Additionally, two of the youngest  $T_{DM2}$  (Hf) ages were determined to be 2.70 and 2.75 Ga, and crustal growth in the NCC around 2.7 Ga has also been confirmed [78,79]. Wan et al. [88] suggested that Anshan's Paleo- to Mesoarchean continental cores were surrounded by continental crust that formed around 2.7 Ga. Monzo- and syenogranites in the Beitai–Waitousha area, with an age of ~2.5 Ga, were produced via partial melting of either ~2.7 Ga juvenile or ~3.5 Ga ancient continent crustal materials [86]. The formation of large granitoid plutons is generally recognized to be influenced by heat and material contributions from the upwelling asthenosphere (e.g., [89,90]). The Lianshanguan syenogranites' positive  $\epsilon_{Hf}$  values and high Mg, Cr, and Ni contents indicate the key role of upwelling asthenosphere in their genesis. Additionally, the metamorphic volcanic rocks of the Anshan Group in the Anshan–Benxi area were formed in the Neoarchean [87,91–93], indicating that younger ~2.7 Ga juvenile crustal materials also contributed to the generation of the Lianshanguan granite.

Compared to the Lianshanguan syenogranites, the Lianshanguan sanukitoid-like granites exhibit characteristics of high-K mafic rocks and metasedimentary sources (Figure 6A–C) and similar formation pressures (7–10 kbar, Figure 6C). However, one Lianshanguan potassium-rich granite has a different source from the tonalites in the  $Al_2O_3/(FeO^T + MgO) - 3CaO - 5K_2O/Na_2O$  diagram (Figure 6A). Therefore, the Lianshanguan granitoids mainly resulted from complex Eoarchean–Neoarchean crustal materials, and extensive syenogranites may have been derived from magmatic mixing processes involving varying proportions of different end-melts.

### 6.3. Reworking of Eoarchean to Mesoarchean Continental Crust in Anshan–Benxi Area

In Northern Liaoning area (north of the Anshan–Benxi area) and Western Liaoning–Eastern Hebei area (west of the Anshan–Benxi area) (Figure 7A), there are abundant late Neoarchean non-tonalite-trondhjemite-granodiorite (non-TTG) granitoids reported [94–100]. Recently, Wang et al. [94] summarized granitoids in the Suizhong granitic belt (which spans the Western Liaoning–Eastern Hebei area) and divided the non-TTG granitoids into two groups, namely sanukitoid-like granites and potassic granites. They suggested that the former resulted from the hybridization of melts from Mesoarchean enriched mafic crust and enriched mantle, whereas the latter resulted from melts from Hadean–Mesoarchean crustal lithologies. In this study, we have rearranged the non-TTG

granitoids from the Suizhong granitic belt ([94]), Northern Liaoning area [98–100], and Anshan–Benxi area ([31,86] and this study). We used the  $f_{\text{Lu}}/\text{Hf} = -0.72$  [58] to recalculate zircon  $T_{\text{DM2}}(\text{Hf})$  values. Non-TTG granitoids were divided into four groups according to the concentrations of  $\text{K}_2\text{O}$  and  $\text{K}_2\text{O}/\text{Na}_2\text{O}$  ratios as follows:

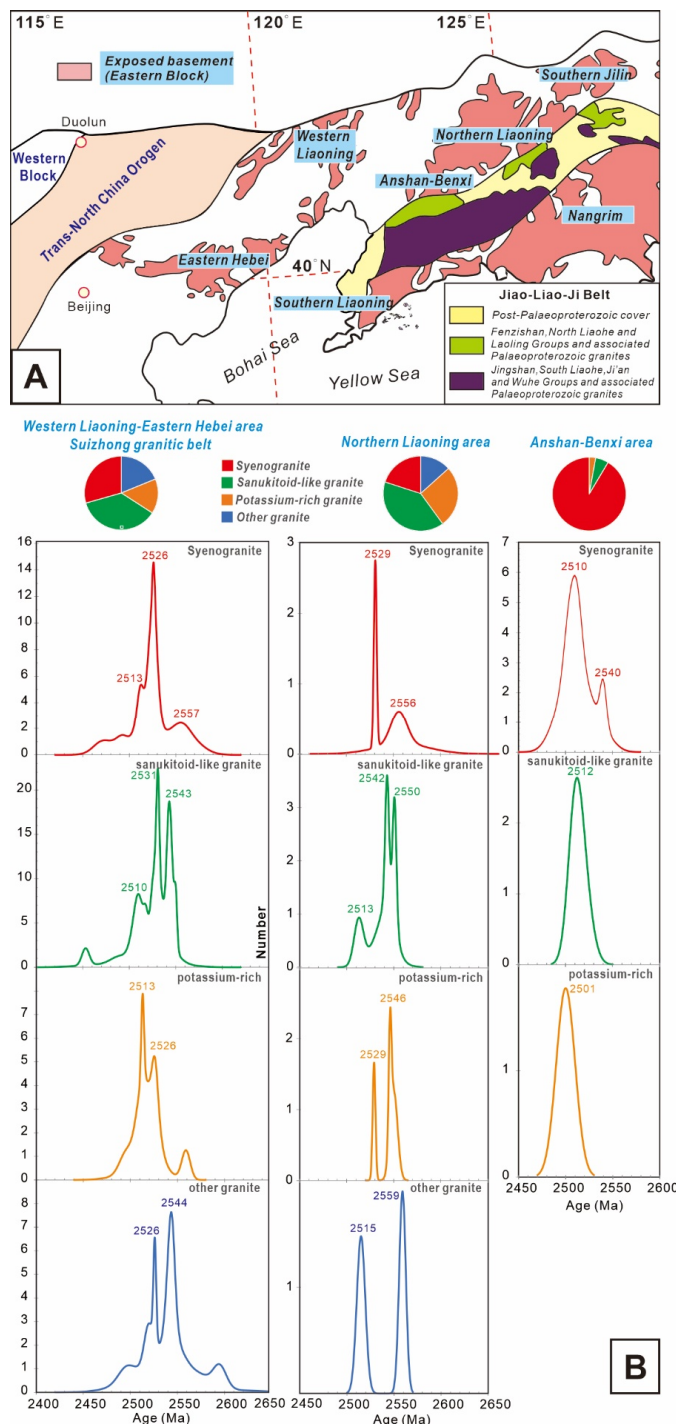


**Figure 7.** (A) Northeastern segment of the Eastern Block (after [30]); (B) Age distributions of ~2.5 Ga syenogranite, sanukitoid-like granite, potassium-rich granites, and other non-TTG granites from the Suizhong granitic belt, Western Liaoning–Eastern Hebei area ([94] and references therein), Northern Liaoning area [98–100], and Anshan–Benxi area ([31,86] and this study).

- Sanukitoid-like granites: They meet most of the sanukitoid criteria defined by Heilimo et al. [77].  $\text{SiO}_2 = 55\text{--}70 \text{ wt. \%}$ ,  $\text{Na}_2\text{O}/\text{K}_2\text{O} = 0.5\text{--}3$ ,  $\text{MgO} = 1.5\text{--}9 \text{ wt. \%}$ ,  $\text{Mg\#} = 45\text{--}65$ ,  $\text{K}_2\text{O} = 1.5\text{--}5.0 \text{ wt. \%}$ ,  $\text{Ba} + \text{Sr} > 1400 \text{ ppm}$ , and  $(\text{Gd}/\text{Er})_{\text{N}} = 2\text{--}6$ .
- Syenogranites: They have  $\text{K}_2\text{O} \geq 4 \text{ wt. \%}$  with  $\text{K}_2\text{O}/\text{Na}_2\text{O} \geq 1.3$  [37].
- Potassium-rich granites: They have  $\text{K}_2\text{O} \geq 4 \text{ wt. \%}$  with  $\text{K}_2\text{O}/\text{Na}_2\text{O} < 1.3$  [37].
- Other granites: They have  $\text{K}_2\text{O} < 4 \text{ wt. \%}$  without sanukitoid-like characteristics.
- Based on the age distribution of the four types of granitoids in different areas (Figure 7B), we observe that the Northern Liaoning area has a higher abundance of sanukitoid-like granites and potassium-rich granites, while the Suizhong granitic belt has more sanukitoid-like granites and syenogranites. In the Anshan–Benxi area, syenogranites make up a significant proportion. The age peaks of these granites range from 2.56 to 2.50 Ga, and no clear age patterns are evident among the four types of granites.

Analyzing the zircon  $T_{\text{DM2}}(\text{Hf})$  values of the four types of granites (Figure 8), we can see that in the Anshan–Benxi area, syenogranites have obvious  $T_{\text{DM2}}(\text{Hf})$  values  $>3.0 \text{ Ga}$ , particularly Eoarchean ages. Most  $T_{\text{DM2}}(\text{Hf})$  ages of the four types of granites from the Northern Liaoning area and Suizhong granitic belt are younger than 3.0 Ga. A weak  $\sim 3.1 \text{ Ga}$   $T_{\text{DM2}}(\text{Hf})$  age peak can also be found in the potassium-rich granites of the Northern Liaoning area and syenogranites of the Suizhong granitic belt.

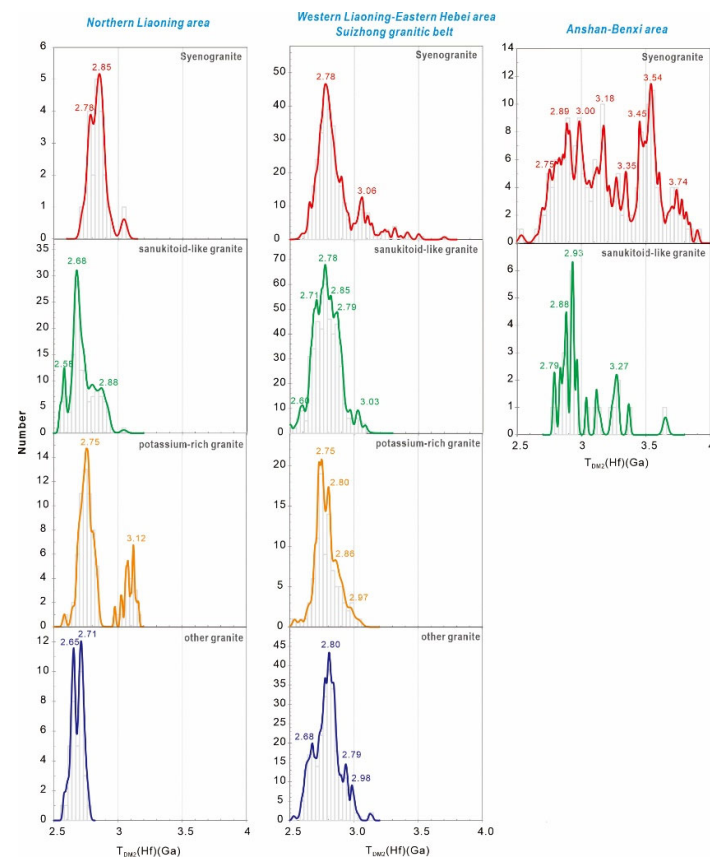


**Figure 8.** Zircon  $T_{\text{DM2}}(\text{Hf})$  age distributions of  $\sim 2.5 \text{ Ga}$  syenogranite, sanukitoid-like granite, potassium-rich granites, and other non-TTG granites from the Suizhong granitic belt, Western Liaoning–Eastern Hebei area ([94]), Northern Liaoning area [98–100], and Anshan–Benxi area ([31,86] and this study). Note: Zircon  $T_{\text{DM2}}(\text{Hf})$  values were recalculated using  $f_{\text{Lu/Hf}} = -0.72$  of the upper continental crustal reservoir [58].

In conclusion, we can infer that older continental crust played an important role in the formation of high  $\text{K}_2\text{O}$  granites. In the Anshan–Benxi area, there was significant

late Neoarchean reworking of the Eoarchean to Mesoarchean continental crust (including metasedimentary sources).

#### 6.4. Tectonic Implications

The advent of late Archean potassic granitoids, as outlined by Laurent et al. [64], symbolizes a pivotal geodynamic transition marked by terrane amalgamation and continental collision. Various studies have supported that the NCC transitioned into an extensional tectonic setting towards the end of the Neoarchean era (~2.52–2.50 Ga) [26,37,101–103]. The manifestation of potassic granitoids, exemplified by the Lianshanguan syenogranites, primarily through the reworking of pre-existing crustal materials, signifies a notable phase in the maturation of the Archean upper continental crust. This large-scale intracrustal recycling of ancient continental materials is indicative of cratonic stability [31].

Wang et al. [98] postulated that a late Neoarchean intra-oceanic arc system existed in the region southwest of Northern Liaoning Terrane and a post-2530 Ma lateral accretion of the Northern Liaoning Terrane to the Anshan–Benxi Terrane occurred. In the Anshan–Benxi area, a back-arc basin evolutionary scenario was also proposed [31,104]. The genesis of Qidashan syenogranites was hypothesized to have occurred during a syntectonic phase where the tectonic regime transitioned from compression to extension within the lower crust. Drawing insights from the investigation of the Suizhong granitic belt, Wang et al. [94] propounded that during the late Archean micro-continent collision (Eastern Hebei and Anshan–Benxi) and post-collisional extension, coupled with the upwelling of the asthenosphere, the pre-existing Archean continental crust was significantly modified and reworked with the production of K-rich granitoids.

Upon juxtaposing ~2.5 Ga syenogranites from the Anshan–Benxi area with those from the Northern Liaoning and Western Liaoning–Eastern Hebei areas, the Anshan–Benxi samples reveal more ancient  $T_{DM2}(Hf)$  ages. This implies a pronounced late Neoarchean reworking of the Eoarchean to Mesoarchean continental crust, primarily in the Anshan–Benxi area. The scenario of arc–continent collision appears to be more plausible.

## 7. Conclusions

1. The Lianshanguan granitoids consist mainly of syenogranites ( $K_2O > 4$  wt. % and  $K_2O/Na_2O$  ratios >1.3). The zircon U–Pb ages of the two syenogranites are  $2541 \pm 22$  and  $2512 \pm 13$  Ma, respectively. These syenogranites have  $\epsilon_{Hf}(t)$  of –20.19 to +4.9, with  $T_{DM2}(Hf)$  ages of 3.90–2.70 Ga.
2. The Lianshanguan syenogranites exhibit similar characteristics to granites derived from meta-sediments. These granites were likely generated from the reworking of Eoarchean–Mesoarchean crustal materials, possibly with a small portion of ~2.7 Ga juvenile crustal materials.
3. Zircon xenocrystic cores indicate two upper intercepts at  $3016 \pm 15$  Ma (MSWD = 1.3, n = 6) and  $3531 \pm 37$  Ma (MSWD = 2.8, n = 5). A metamorphic age of  $1919 \pm 85$  Ma (MSWD = 20, n = 9) was also obtained.
4. Compared to the  $T_{DM2}(Hf)$  ages of late Neoarchean syenogranites from the Anshan–Benxi area (prominent peaks at 3.54, 3.45, and 2.89 Ga and subordinate age peaks at 3.79, 3.74, 3.34, and 3.02 Ga), the  $T_{DM2}(Hf)$  ages of late Neoarchean syenogranites from Northern Liaoning and Western Liaoning–Eastern Hebei areas show one dominant peak at ~2.8 Ga and one subordinate age peak at ~3.1 Ga, indicating that the late Neoarchean reworking of the Eoarchean to Paleoarchean continental crust mainly occurred in the Anshan–Benxi area.
5. An arc–continent collision is likely the dominant geodynamic mechanism during the late Neoarchean.

**Supplementary Materials:** The following supporting information can be downloaded at <https://www.mdpi.com/article/10.3390/min1410005/s1>. Figure S1: Bivariate plots; Table S1: LA-ICP-MS zircon U–Pb analyses of Lianshanguan syenogranites, Anshan–Benxi area; Table S2:

Zircon Hf analyses for Lianshanguan syenogranites, Anshan–Benxi area; Table S3: Whole-rock major (wt. %) and trace (ppm) element data for Lianshanguan syenogranites, Anshan–Benxi area.

**Author Contributions:** W.Z.: Data curation, Writing—original draft preparation, review and editing, Visualization, and Funding acquisition; W.W.: Supervision, Writing—review and editing, and Visualization; L.D.: Supervision, Data curation, and Writing—review and editing; P.L.: Investigation, Supervision, Writing—review and editing, and Funding acquisition; W.X.: Writing—review and editing and Funding acquisition. All authors have read and agreed to the published version of the manuscript.

**Funding:** This research was funded by the Chinese Geological Survey Bureau project (grant numbers DD20230209 and DD20221645), National Natural Science Foundation of China (grant numbers 42272232 and 41972205) and China Postdoctoral Science Foundation (2019M660743).

**Data Availability Statement:** Data is contained within the article.

**Conflicts of Interest:** The authors declare no conflict of interest. The funders had no role in the design of the study, collection, analyses, or interpretation of data, writing of the manuscript, or decision to publish the results.

## References

- Bell, E.A.; Harrison, T.M.; McCulloch, M.T.; Young, E.D. Early Archean crustal evolution of the Jack Hills Zircon source terrane inferred from Lu–Hf, 207Pb/206Pb, and  $\delta^{18}\text{O}$  systematics of Jack Hills zircons. *Geochim. Cosmochim. Acta* **2011**, *75*, 4816–4829. [[CrossRef](#)]
- Cui, P.; Sun, J.; Sha, D.; Wang, X.; Zhang, P.; Gu, A.; Wang, Z. Oldest zircon xenocryst (4.17 Ga) from the north China craton. *Int. Geol. Rev.* **2013**, *55*, 1902–1908. [[CrossRef](#)]
- Diwu, C.; Sun, Y.; Wilde, S.A.; Wang, H.; Dong, Z.; Zhang, H.; Wang, Q. New evidence for ~4.45 Ga terrestrial crust from zircon xenocrysts in Ordovician ignimbrite in the North Qinling Orogenic Belt, China. *Gondwana Res.* **2013**, *23*, 1484–1490. [[CrossRef](#)]
- Furnes, H.; Rosing, M.; Dilek, Y.; de Wit, M. Isua supracrustal belt (Greenland)—A vestige of a 3.8 Ga suprasubduction zone ophiolite, and the implications for Archean geology. *Lithos* **2009**, *113*, 115–132. [[CrossRef](#)]
- Harrison, T.M. The Hadean crust: Evidence from >4 Ga zircons. *Annu. Rev. Earth Planet. Sci.* **2009**, *37*, 479–505. [[CrossRef](#)]
- Iizuka, T.; Horie, K.; Komiya, T.; Maruyama, S.; Hirata, T.; Hidaka, H.; Windley, B.F. 4.2 Ga zircon xenocryst in an Acosta gneiss from northwestern Canada: Evidence for early continental crust. *Geology* **2006**, *34*, 245–248. [[CrossRef](#)]
- Iizuka, T.; Komiya, T.; Johnson, S.P.; Kon, Y.; Maruyama, S.; Hirata, T. Reworking of Hadean crust in the Acosta gneisses, northwestern Canada: Evidence from in-situ Lu–Hf isotope analysis of zircon. *Chem. Geol.* **2009**, *259*, 230–239. [[CrossRef](#)]
- Kemp, A.; Wilde, S.; Hawkesworth, C.; Coath, C.; Nemchin, A.; Pidgeon, R.; Vervoort, J.; DuFrane, S. Hadean crustal evolution revisited: New constraints from Pb–Hf isotope systematics of the Jack Hills zircons. *Earth Planet. Sci. Lett.* **2010**, *296*, 45–56. [[CrossRef](#)]
- Liu, D.; Nutman, A.P.; Compston, W.; Wu, J.; Shen, Q. Remnants of  $\geq 3800$  Ma crust in the Chinese part of the Sino-Korean Craton. *Geology* **1992**, *20*, 339–342. [[CrossRef](#)]
- Liu, D.; Wilde, S.A.; Wan, Y.; Wu, J.; Zhou, H.; Dong, C.; Yin, X. New U–Pb and Hf isotopic data confirm Anshan as the oldest preserved segment of the North China Craton. *Am. J. Sci.* **2008**, *308*, 200–231. [[CrossRef](#)]
- Maniar, P.D.; Piccoli, P.M. Tectonic discrimination of granitoids. *Geol. Soc. Am. Bull.* **1989**, *101*, 635–643. [[CrossRef](#)]
- Mojzsis, S.J.; Harrison, T.M. Establishment of a 3.83-Ga magmatic age for the Akilia tonalite (southern West Greenland). *Earth Planet. Sci. Lett.* **2002**, *202*, 563–576. [[CrossRef](#)]
- Naeraa, T.; Scherstén, A.; Rosing, M.; Kemp, A.; Hoffmann, J.; Kokfelt, T.; Whitehouse, M. Hafnium isotope evidence for a transition in the dynamics of continental growth 3.2 Gyr ago. *Nature* **2012**, *485*, 627–630. [[CrossRef](#)] [[PubMed](#)]
- Nutman, A.P.; Friend, C.R.; Horie, K.; Hidaka, H. The Itsaq Gneiss Complex of southern West Greenland and the construction of Eoarchean crust at convergent plate boundaries. *Dev. Precambrian Geol.* **2007**, *15*, 187–218.
- O’Neil, J.; Carlson, R.W.; Francis, D.; Stevenson, R.K. Neodymium-142 evidence for Hadean mafic crust. *Science* **2008**, *321*, 1828–1831. [[CrossRef](#)]
- Paquette, J.-L.; Barbosa, J.; Rohais, S.; Cruz, S.; Goncalves, P.; Peucat, J.-J.; Leal, A.; Santos-Pinto, M.; Martin, H. The geological roots of South America: 4.1 Ga and 3.7 Ga zircon crystals discovered in NE Brazil and NW Argentina. *Precambrian Res.* **2015**, *271*, 49–55. [[CrossRef](#)]
- Vervoort, J.D.; Kemp, A.I. Clarifying the zircon Hf isotope record of crust–mantle evolution. *Chem. Geol.* **2016**, *425*, 65–75. [[CrossRef](#)]
- Wan, Y.; Liu, D.; Dong, C.Y.; Nutman, A.; Wilde, S.A.; Wang, W.; Xie, H.; Yin, X.; Zhou, H. The oldest rocks and zircons in China. *Acta Petrol. Sin.* **2009**, *25*, 1793–1807, (In Chinese with English abstract).
- Wilde, S.A.; Valley, J.W.; Peck, W.H.; Graham, C.M. Evidence from detrital zircons for the existence of continental crust and oceans on the Earth 4.4 Gyr ago. *Nature* **2001**, *409*, 175–178. [[CrossRef](#)]

20. Zeh, A.; Gerdes, A.; Klemd, R.; Barton, J., Jr. U–Pb and Lu–Hf isotope record of detrital zircon grains from the Limpopo Belt—evidence for crustal recycling at the Hadean to early-Archean transition. *Geochim. Et Cosmochim. Acta* **2008**, *72*, 5304–5329. [[CrossRef](#)]
21. Tolstikhin, I.N.; Kramers, J.D. *The Evolution of Matter—From the Big Bang to the Present Day*; Cambridge University Press: Cambridge, UK, 2008.
22. Wan, Y.; Xie, H.; Wang, H.; Liu, S.; Chu, H.; Xiao, Z.; Li, Y.; Hao, G.; Li, P.; Dong, C.; et al. Discovery of early Eoarchean-Hadean zircons in eastern Hebei, North China Craton. *Acta Geol. Sin.* **2021**, *95*, 277–291, (In Chinese with English abstract).
23. Wan, Y.; Liu, D.; Dong, C.; Xie, H.; Kröner, A.; Ma, M.; Liu, S.; Xie, S.; Ren, P. Formation and evolution of Archean continental crust of the North China Craton. In *Precambrian Geology of China*; Springer: Berlin/Heidelberg, Germany, 2015; pp. 59–136.
24. Wan, Y.; Xie, H.; Dong, C.; Kröner, A.; Wilde, S.A.; Bai, W.; Liu, S.; Xie, S.; Ma, M.; Li, Y.; et al. Chapter 14—Hadean to Paleoarchean Rocks and Zircons in China. In *Earth's Oldest Rocks*, 2nd ed.; Van Kranendonk, M.J., Bennett, V.C., Hoffmann, J.E., Eds.; Elsevier: Berlin, Germany, 2019; pp. 293–327.
25. Yuan, W.; Yang, Z.; Yang, J. The discovery of hadean detrital zircon in late Devonian strata in Hexi corridor, Northwest China. *Acta Petrol. Sin.* **2012**, *28*, 1029–1036. (In Chinese with English abstract)
26. Nutman, A.P.; Wan, Y.; Du, L.; Friend, C.R.L.; Dong, C.; Xie, H.; Wang, W.; Sun, H.; Liu, D. Multistage late Neoarchaean crustal evolution of the North China Craton, eastern Hebei. *Precambrian Res.* **2011**, *189*, 43–65. [[CrossRef](#)]
27. Sun, G.; Liu, S.; Cawood, P.A.; Tang, M.; van Hunen, J.; Gao, L.; Hu, Y.; Hu, F. Thermal state and evolving geodynamic regimes of the Meso- to Neoarchean North China Craton. *Nat. Commun.* **2021**, *12*, 3888. [[CrossRef](#)] [[PubMed](#)]
28. Zhai, M.; Santosh, M. The early Precambrian odyssey of the North China Craton: A synoptic overview. *Gondwana Res.* **2011**, *20*, 6–25. [[CrossRef](#)]
29. Zhao, G.; Zhai, M. Lithotectonic elements of Precambrian basement in the North China Craton: Review and tectonic implications. *Gondwana Res.* **2013**, *23*, 1207–1240. [[CrossRef](#)]
30. Zhao, G.; Sun, M.; Wilde, S.A.; Li, S. Late Archean to Paleoproterozoic evolution of the North China Craton: Key issues revisited. *Precambrian Res.* **2005**, *136*, 177–202. [[CrossRef](#)]
31. Wan, Y.; Ma, M.; Dong, C.; Xie, H.; Xie, S.; Ren, P.; Liu, D. Widespread late neoarchean reworking of Meso- to paleoarchean continental crust in the Anshan-Benxi area, North China Craton, as documented by U-Pb-Nd-Hf-O isotopes. *Am. J. Sci.* **2015**, *315*, 620–670. [[CrossRef](#)]
32. LBGMR (Liaoning Bureau of Geology and Mineral Resources). *1/200,000 Geological Map of Yingkou City and Liaoyang*; Geological Survey Report; LBGMR: Jinxian, China, 1975.
33. Yang, F.; Sun, J.; Song, Y.; Zhang, P.; Bi, Z. SHRIMP U-Pb Age, Hf Isotope Composition and Geochemical Characteristics of Neoarchean Granitic Complex in Liaodong Lianshanguan Area, NE China. *Earth Sci.* **2016**, *41*, 2008–2018. (In Chinese with English abstract)
34. Song, B.; Nutman, A.P.; Liu, D.; Wu, J. 3800 to 2500 Ma crustal evolution in the Anshan area of Liaoning Province, northeastern China. *Precambrian Res.* **1996**, *78*, 79–94. [[CrossRef](#)]
35. Wan, Y.; Liu, D.; Song, B.; Wu, J.; Yang, C.; Zhang, Z.; Geng, Y. Geochemical and Nd isotopic compositions of 3.8 Ga meta-quartz dioritic and trondhjemite rocks from the Anshan area and their geological significance. *J. Asian Earth Sci.* **2005**, *24*, 563–575. [[CrossRef](#)]
36. Wan, Y.; Song, B.; Geng, Y.; Liu, D. Geochemical characteristics of Archaean basement in the Fushun-Qingyuan area, northern Liaoning Province and its geological significance. *Geol. Rev.* **2005**, *51*, 128–137.
37. Wan, Y.; Dong, C.; Liu, D.; Kröner, A.; Yang, C.; Wang, W.; Du, L.; Xie, H.; Ma, M. Zircon ages and geochemistry of late Neoarchean syenogranites in the North China Craton: A review. *Precambrian Res.* **2012**, *222–223*, 265–289. [[CrossRef](#)]
38. Wang, Y.; Li, X.; Jin, W.; Zhang, J. Eoarchean ultra-depleted mantle domains inferred from ca. 3.81Ga Anshan trondhjemite gneisses, North China Craton. *Precambrian Res.* **2015**, *263*, 88–107. [[CrossRef](#)]
39. Dong, C.; Wan, Y.; Xie, H.; Nutman, A.P.; Xie, S.; Liu, S.; Ma, M.; Liu, D. The Mesoarchean Tiejiashan-Gongchangling potassio granite in the Anshan-Benxi area, North China Craton: Origin by recycling of Paleo-to Eoarchean crust from U-Pb-Nd-Hf-O isotopic studies. *Lithos* **2017**, *290*, 116–135. [[CrossRef](#)]
40. Bao, H.; Liu, S.; Wang, M.; Teng, G.; Sun, G. Mesoarchean geodynamic regime evidenced from diverse granitoid rocks in the Anshan-Benxi area of the North China Craton. *Lithos* **2020**, *366–367*, 105574. [[CrossRef](#)]
41. Wang, Y.; Li, X.; Jin, W.; Zeng, L.; Zhang, J. Generation and maturation of Mesoarchean continental crust in the Anshan Complex, North China Craton. *Precambrian Res.* **2020**, *341*, 105651. [[CrossRef](#)]
42. Wan, Y.; Dong, C.; Xie, H.; Nutman, A.P.; Xie, S.; Wang, Y.; Liu, D. SHRIMP U-Pb zircon dating and geochemistry of the 3.8–3.1 Ga Hujiamiao Complex in Anshan (North China Craton) and the significance of the trondhjemites for early crustal genesis. *Precambrian Res.* **2023**, *388*, 106975. [[CrossRef](#)]
43. Wu, J.S.; Geng, Y.S.; Shen, Q.H.; Wan, Y.S.; Liu, D.Y.; Song, B. *Archean Geology: Characterization and Tectonic Evolution of China-Korea Paleo-Continent*; Geological Publishing House: Beijing, China, 1998. (In Chinese with English abstract)
44. Wu, F.; Zhang, Y.; Yang, J.; Xie, L.; Yang, Y. Zircon U-Pb and Hf isotopic constraints on the Early Archean crustal evolution in Anshan of the North China Craton. *Precambrian Res.* **2008**, *167*, 339–362. [[CrossRef](#)]
45. LBGMR (Liaoning Bureau of Geology and Mineral Resources). *1/250,000 Geological Map of Dandong City and Donggang City*; Geological Survey Report; LBGMR: Liaoning, China, 2003. (In Chinese)

46. Wu, D.; Zhuang, T.; Liu, X.; Wang, C. Petrological and geochemical characteristics of remelting chorismite in Lianshanguan area of east Liaoning. *World Nucl. Geosci.* **2013**, *30*, 210–216. (In Chinese with English abstract)
47. Wu, D. Early Precambrian Tectonic Evolution and Uranium Mineralization in Lianshanguan Area, Eastern Liaoning Province. Ph.D. Thesis, Jilin University, Changchun, China, 2021. (In Chinese with English abstract)
48. Zong, K.; Zhang, Z.; He, Z.; Hu, Z.; Santosh, M.; Liu, Y.; Wang, W. Early Palaeozoic high-pressure granulites from the Dunhuang block, northeastern Tarim Craton: Constraints on continental collision in the southern Central Asian Orogenic Belt. *J. Metamorph. Geol.* **2012**, *30*, 753–768. [[CrossRef](#)]
49. Sláma, J.; Košler, J.; Condon, D.J.; Crowley, J.L.; Gerdes, A.; Hanchar, J.M.; Horstwood, M.S.; Morris, G.A.; Nasdala, L.; Norberg, N. Plešovice zircon—A new natural reference material for U–Pb and Hf isotopic microanalysis. *Chem. Geol.* **2008**, *249*, 1–35. [[CrossRef](#)]
50. Jackson, S.E.; Pearson, N.J.; Griffin, W.L.; Belousova, E.A. The application of laser ablation-inductively coupled plasma-mass spectrometry to in situ U–Pb zircon geochronology. *Chem. Geol.* **2004**, *211*, 47–69. [[CrossRef](#)]
51. Liu, Y.; Hu, Z.; Gao, S.; Günther, D.; Xu, J.; Gao, C.; Chen, H. In situ analysis of major and trace elements of anhydrous minerals by LA-ICP-MS without applying an internal standard. *Chem. Geol.* **2008**, *257*, 34–43. [[CrossRef](#)]
52. Liu, Y.; Gao, S.; Hu, Z.; Gao, C.; Zong, K.; Wang, D. Continental and Oceanic Crust Recycling-induced Melt–Peridotite Interactions in the Trans-North China Orogen: U–Pb Dating, Hf Isotopes and Trace Elements in Zircons from Mantle Xenoliths. *J. Petrol.* **2010**, *51*, 392–399. [[CrossRef](#)]
53. Ludwig, K.R. Isoplot 3.0: A geochronological toolkit for Microsoft excel. *Berkeley Geochronol. Cent. Spec. Publ.* **2003**, *4*, 1–71.
54. Belousova, E.A.; Griffin, W.L.; O'Reilly, S.Y.; Fisher, N.I. Igneous zircon: Trace element composition as an indicator of source rock type. *Contrib. Mineral. Petrol.* **2002**, *143*, 602–622. [[CrossRef](#)]
55. Corfu, F.; Hanchar, J.M.; Hoskin, P.W.O.; Kinny, P. Atlas of zircon textures. *Rev. Mineral. Geochem.* **2003**, *53*, 469–500. [[CrossRef](#)]
56. Tomaszek, F.; Kennedy, A.K.; Villa, I.M.; Lagos, M.; Ballhaus, C. Zircons from Syros, Cyclades, Greece—Recrystallization and Mobilization of Zircon During High-Pressure Metamorphism. *J. Petrol.* **2003**, *44*, 1977–2002. [[CrossRef](#)]
57. Sun, S.S.; McDonough, W.F. Chemical and isotopic systematics of oceanic basalts: Implications for mantle composition and processes. *Geol. Soc. Spec. Publ.* **1989**, *42*, 313–345. [[CrossRef](#)]
58. Amelin, Y.; Lee, D.-C.; Halliday, A.N.; Pidgeon, R.T. Nature of the Earth's earliest crust from hafnium isotopes in single detrital zircons. *Nature* **1999**, *399*, 252–255. [[CrossRef](#)]
59. Griffin, W.L.; O'Reilly, S.Y.; Abe, N.; Aulbach, S.; Davies, R.M.; Pearson, N.J.; Doyle, B.J.; Kivi, K. The origin and evolution of Archean lithospheric mantle. *Precambrian Res.* **2003**, *127*, 19–41. [[CrossRef](#)]
60. Streckeisen, A. To each plutonic rock its proper name. *Earth-Sci. Rev.* **1976**, *12*, 1–33. [[CrossRef](#)]
61. Frost, B.R.; Barnes, C.G.; Collins, W.J.; Arculus, R.J.; Ellis, D.J.; Frost, C.D. A geochemical classification for granitic rocks. *J. Petrol.* **2001**, *42*, 2033–2048. [[CrossRef](#)]
62. Rollinson, H.R. *Using Geochemical Data, Evaluation, Presentation, Interpretation*; John Wiley & Sons. Inc.: New York, NY, USA, 1993.
63. Moyen, J.F.; Martin, H.; Jayananda, M.; Auvray, B. Late Archaean granites: A typology based on the Dharwar Craton (India). *Precambrian Res.* **2003**, *127*, 103–123. [[CrossRef](#)]
64. Laurent, O.; Martin, H.; Moyen, J.F.; Doucelance, R. The diversity and evolution of late-Archean granitoids: Evidence for the onset of “modern-style” plate tectonics between 3.0 and 2.5 Ga. *Lithos* **2014**, *205*, 208–235. [[CrossRef](#)]
65. Li, S.; Zhao, G. SHRIMP U–Pb zircon geochronology of the Liaoji granitoids: Constraints on the evolution of the Paleoproterozoic Jiao-Liao-Ji belt in the Eastern Block of the North China Craton. *Precambrian Res.* **2007**, *158*, 1–16. [[CrossRef](#)]
66. Li, S.; Zhao, G.; Sun, M.; Han, Z.; Luo, Y.; Hao, D.; Xia, X. Deformation history of the Paleoproterozoic Liaohe assemblage in the eastern block of the North China Craton. *J. Asian Earth Sci.* **2005**, *24*, 659–674. [[CrossRef](#)]
67. Li, S.; Zhao, G.; Sun, M.; Han, Z.; Zhao, G.; Hao, D. Are the South and North Liaohe Groups of North China Craton different exotic terranes? Nd isotope constraints. *Gondwana Res.* **2006**, *9*, 198–208. [[CrossRef](#)]
68. Liu, F.; Wang, F.; Liu, P.; Liu, C. Multiple metamorphic events revealed by zircons from the Diancang Shan-Ailao Shan metamorphic complex, southeastern Tibetan Plateau. *Gondwana Res.* **2013**, *24*, 429–450. [[CrossRef](#)]
69. Liu, P.; Liu, F.; Cai, J.; Wang, F.; Liu, C.; Liu, J.; Yang, H.; Shi, J.; Liu, L. Discovery and geological significance of high-pressure mafic granulites in the Pingdu–Anqiu area of the Jiaobei Terrane, the Jiao–Liao–Ji Belt, the North China Craton. *Precambrian Res.* **2017**, *303*, 445–469. [[CrossRef](#)]
70. Luo, Y.; Sun, M.; Zhao, G.; Li, S.; Xu, P.; Ye, K.; Xia, X. LA-ICP-MS U–Pb zircon ages of the Liaohe Group in the Eastern Block of the North China Craton: Constraints on the evolution of the Jiao-Liao-Ji Belt. *Precambrian Res.* **2004**, *134*, 349–371. [[CrossRef](#)]
71. Luo, Y.; Sun, M.; Zhao, G.; Li, S.; Ayers, J.C.; Xia, X.; Zhang, J. A comparison of U–Pb and Hf isotopic compositions of detrital zircons from the North and South Liaohe Groups: Constraints on the evolution of the Jiao-Liao-Ji Belt, North China Craton. *Precambrian Res.* **2008**, *163*, 279–306. [[CrossRef](#)]
72. Meng, E.; Wang, C.Y.; Li, Z.; Li, Y.-G.; Yang, H.; Cai, J.; Ji, L.; Jin, M.Q. Palaeoproterozoic metasedimentary rocks of the Ji'an Group and their significance for the tectonic evolution of the northern segment of the Jiao–Liao–Ji Belt, North China Craton. *Geol. Mag.* **2018**, *155*, 149–173. [[CrossRef](#)]
73. Tam, P.Y.; Zhao, G.; Liu, F.; Zhou, X.; Sun, M.; Li, S. Timing of metamorphism in the Paleoproterozoic Jiao-Liao-Ji Belt: New SHRIMP U–Pb zircon dating of granulites, gneisses and marbles of the Jiaobei massif in the North China Craton. *Gondwana Res.* **2011**, *19*, 150–162. [[CrossRef](#)]

74. Zhou, X.; Zhao, G.; Wei, C.; Geng, Y.; Sun, M. EPMA U-Th-Pb monazite and SHRIMP U-Pb zircon geochronology of high-pressure pelitic granulites in the Jiaobei massif of the North China Craton. *Am. J. Sci.* **2008**, *308*, 328–350. [[CrossRef](#)]
75. LBGMR (Liaoning Bureau of Geology and Mineral Resources). Regional geology of Liaoning Province. In *Regional Geology of China*; Li, T.D., Ed.; Geological Publishing House: Beijing, China, 2017.
76. Zhang, K.J. Destruction of the North China Craton: Lithosphere folding-induced removal of lithospheric mantle? *J. Geodyn.* **2012**, *53*, 8–17. [[CrossRef](#)]
77. Heilimo, E.; Halla, J.; Hölttä, P. Discrimination and origin of the sanukitoid series: Geochemical constraints from the Neoarchean western Karelian Province (Finland). *Lithos* **2010**, *115*, 27–39. [[CrossRef](#)]
78. Altherr, R.; Holl, A.; Hegner, E.; Langer, C.; Kreuzer, H. High-potassium, calc-alkaline I-type plutonism in the European Variscides: Northern Vosges (France) and northern Schwarzwald (Germany). *Lithos* **2000**, *50*, 51–73. [[CrossRef](#)]
79. Schiano, P.; Monzier, M.; Eissen, J.P.; Martin, H.; Koga, K.T. Simple mixing as the major control of the evolution of volcanic suites in the Ecuadorian Andes. *Contrib. Mineral. Petrol.* **2010**, *160*, 297–312. [[CrossRef](#)]
80. Patiño Douce, A.E.; Johnston, A.D. Phase equilibria and melt productivity in the pelitic system: Implications for the origin of peraluminous granitoids and aluminous granulites. *Contrib. Mineral. Petrol.* **1991**, *107*, 202–218. [[CrossRef](#)]
81. Skjerlie, K.P.; Johnston, A.D. Vapour-absent melting from 10 to 20 kbar of crustal rocks that contain multiple hydrous phases: Implications for anatexis in the deep to very deep continental crust and active continental margins. *J. Petrol.* **1996**, *37*, 661–691. [[CrossRef](#)]
82. Watson, E.B.; Harrison, T.M. Zircon saturation revisited: Temperature and composition effects in a variety of crustal magma types. *Earth Planet. Sci. Lett.* **1983**, *64*, 295–304. [[CrossRef](#)]
83. Whalen, J.B.; Currie, K.L.; Chappell, B.W. A-type granites: Geochemical characteristics, discrimination and petrogenesis. *Contrib. Mineral. Petrol.* **1987**, *95*, 407–419. [[CrossRef](#)]
84. Chappell, B.W. Aluminium saturation in I- and S-type granites and the characterization of fractionated haplogranites. *Lithos* **1999**, *46*, 535–551. [[CrossRef](#)]
85. Clemens, J.D. S-type granitic magmas—Petrogenetic issues, models and evidence. *Earth-Sci. Rev.* **2003**, *61*, 1–18. [[CrossRef](#)]
86. Liu, S.; Wang, M.; Wan, Y.; Guo, R.; Wang, W.; Wang, K.; Guo, B.; Fu, J.; Hu, F. A reworked ~3.45 Ga continental microblock of the North China Craton: Constraints from zircon U-Pb-Lu-Hf isotopic systematics of the Archean Beital-Waitoushan migmatite-syenogranite complex. *Precambrian Res.* **2017**, *303*, 332–354. [[CrossRef](#)]
87. Dai, Y.; Zhang, L.; Zhu, M.; Wang, C.; Liu, L.; Xiang, P. The composition and genesis of the Mesoarchean Dagushan banded iron formation (BIF) in the Anshan area of the North China Craton. *Ore Geol. Rev.* **2014**, *63*, 353–373. [[CrossRef](#)]
88. Wan, Y.; Xie, S.; Yang, C.; Kröner, A.; Ma, M.; Dong, C.; Du, L.; Xie, H.; Liu, D. Early Neoarchean (~2.7 Ga) tectono-thermal events in the North China Craton: A synthesis. *Precambrian Res.* **2014**, *247*, 45–63. [[CrossRef](#)]
89. Thompson, A.B.; Connolly, J.A.D. Melting of the continental crust: Some thermal and petrological constraints on anatexis in continental collision zones and other tectonic settings. *J. Geophys. Res.* **1995**, *100*, 15565–15579. [[CrossRef](#)]
90. Lu, L.; Zhang, K.J.; Yan, L.L.; Jin, X.; Zhang, Y.X. Was Late Triassic Tanggula granitoid (central Tibet, western China) a product of melting of underthrust Songpan-Ganzi flysch sediments? *Tectonics* **2017**, *36*, 902–928. [[CrossRef](#)]
91. Han, C.; Xiao, W.; Su, B.-X.; Sakai, P.A.; Chen, Z.; Zhang, X.; Ao, S.; Zhang, J.; Wan, B.; Zhang, Z.; et al. Formation age and genesis of the Gongchangling Neoarchean banded iron deposit in eastern Liaoning Province: Constraints from geochemistry and SHRIMP zircon U-Pb dating. *Precambrian Res.* **2014**, *254*, 306–322. [[CrossRef](#)]
92. Fan, Z.; Huang, X.; Tan, L.; Yang, X.; Zhang, H.; Zhou, D.; Liu, Q.; Cao, B. A study of iron deposits in the Anshan area, China based on interactive inversion technique of gravity and magnetic anomalies. *Ore Geol. Rev.* **2014**, *57*, 618–627. [[CrossRef](#)]
93. Guo, R.; Liu, S.; Gong, E.; Wang, W.; Wang, M.; Fu, J.; Qin, T. Arc-generated metavolcanic rocks in the Anshan–Benxi greenstone belt, North China Craton: Constraints from geochemistry and zircon U-Pb–Hf isotopic systematics. *Precambrian Res.* **2017**, *303*, 228–250. [[CrossRef](#)]
94. Wang, C.; Song, S.; Su, L.; Allen, M.B. Crustal maturation and cratonization in response to Neoarchean continental collision: The Suizhong granitic belt, North China Craton. *Precambrian Res.* **2022**, *377*, 106732. [[CrossRef](#)]
95. Fu, J.; Liu, S.; Wang, M.; Chen, X.; Guo, B.; Hu, F. Late Neoarchean monzogranitic–syenogranitic gneisses in the Eastern Hebei–Western Liaoning Province, North China Craton: Petrogenesis and implications for tectonic setting. *Precambrian Res.* **2017**, *303*, 392–413. [[CrossRef](#)]
96. Fu, J.; Liu, S.; Cawood, P.A.; Wang, M.; Hu, F.; Sun, G.; Gao, L.; Hu, Y. Neoarchean magmatic arc in the Western Liaoning Province, northern North China Craton: Geochemical and isotopic constraints from sanukitoids and associated granitoids. *Lithos* **2018**, *322*, 296–311. [[CrossRef](#)]
97. Fu, J.; Liu, S.; Zhang, B.; Guo, R.; Wang, M. A Neoarchean K-rich granitoid belt in the northern North China Craton. *Precambrian Res.* **2019**, *328*, 193–216. [[CrossRef](#)]
98. Wang, W.; Cawood, P.A.; Liu, S.; Guo, R.; Bai, X.; Wang, K. Cyclic formation and stabilization of Archean lithosphere by accretionary orogenesis: Constraints from TTG and potassic granitoids, North China Craton. *Tectonics* **2017**, *36*, 1724–1742. [[CrossRef](#)]
99. Wang, K.; Liu, S.; Wang, M.; Yan, M. Geochemistry and zircon U-Pb-Hf isotopes of the late Neoarchean granodiorite-monzogranite-quartz syenite intrusions in the Northern Liaoning Block, North China Craton: Petrogenesis and implications for geodynamic processes. *Precambrian Res.* **2017**, *295*, 151–171. [[CrossRef](#)]

100. Cheng, C.; Liu, J.; Zhang, J.; Chen, Y.; Yin, C.; Liu, X.; Qian, J.; Gao, P.; Wang, X. Petrogenesis of newly identified Neoarchean granitoids in the Qingyuan of NE China: Implications on crustal growth and reworking of the North China Craton. *J. Asian Earth Sci.* **2022**, *236*, 105333. [[CrossRef](#)]
101. Zhao, G.; Wilde, S.A.; Cawood, P.A.; Lu, L. Thermal evolution of two textural types of mafic granulites in the North China craton: Evidence for both mantle plume and collisional tectonics. *Geol. Mag.* **1999**, *136*, 223–240. [[CrossRef](#)]
102. Yang, J.; Wu, F.; Wilde, S.A.; Zhao, G. Petrogenesis and geodynamics of Late Archean magmatism in eastern Hebei, eastern North China Craton: Geochronological, geochemical and Nd–Hf isotopic evidence. *Precambrian Res.* **2008**, *167*, 125–149. [[CrossRef](#)]
103. Wan, Y.; Liu, D.; Wang, S.; Dong, C.; Yang, E.; Wang, W.; Zhou, H.; Ning, Z.; Du, L.; Yin, X. Juvenile magmatism and crustal recycling at the end of the Neoarchean in Western Shandong Province, North China Craton: Evidence from SHRIMP zircon dating. *Am. J. Sci.* **2010**, *310*, 1503–1552. [[CrossRef](#)]
104. Wan, Y. *The Formation and Evolution of the Iron-Bearing Rock Series of the Gongchangling Area, Liaoning Province*; Beijing Science and Technology Publishing House: Beijing, China, 1993; pp. 1–108.

**Disclaimer/Publisher’s Note:** The statements, opinions and data contained in all publications are solely those of the individual author(s) and contributor(s) and not of MDPI and/or the editor(s). MDPI and/or the editor(s) disclaim responsibility for any injury to people or property resulting from any ideas, methods, instructions or products referred to in the content.